

ANALYSING SPATIAL DATA VIA GEOSTATISTICAL METHODS

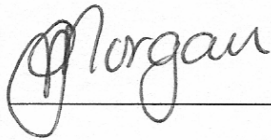
Craig John Morgan

A dissertation submitted to the Faculty of Science, University of the Witwatersrand, Johannesburg, in fulfillment of the requirements for the degree of Master of Science.

Johannesburg, 2005

DECLARATION

I declare that this dissertation is my own, unaided work. It is being submitted for the Degree of Master of Science at the University of the Witwatersrand, Johannesburg. It has not been submitted before for any degree or examination in any other University.

 _____

5th day of December 2005

ABSTRACT

This dissertation presents a detailed study of geostatistics. Included in this work are details of the development of geostatistics and its usefulness both in and outside of the mining industry, a comprehensive presentation of the theory of geostatistics, and a discussion of the application of this theory to practical situations. A published debate over the validity of geostatistics is also examined.

The ultimate goal of this dissertation is to provide a thorough investigation of geostatistics from both a theoretical and a practical perspective. The theory presented in this dissertation is thus tested on various spatial data sets, and from these tests it is concluded that geostatistics can be effectively used in practice provided that the practitioner fully understands the theory of geostatistics and the spatial data being analyzed. A particularly interesting conclusion to come out of this dissertation is the importance of using additive regionalized variables in all geostatistical analyses.

ACKNOWLEDGEMENTS

First of all, I wish to express thanks to my two supervisors, Professor Paul Fatti and Professor Dick Minnitt, for their assistance over the past three years. I would also like to thank Christina Dohm for supplying a sizeable spatial data set taken from the South African gold mining industry, and for allowing me to attend the three courses

1. Statistical Valuation of Ore Reserves (MINN 511)
2. Geostatistical Evaluation of Mineral Resources (MINN 510)
3. Practical Implementation of Geostatistical Evaluation (MINN 572)

given at the University of the Witwatersrand in 2003. Special thanks also goes out to Isobel Clark for making available the geostatistical computer package Geostokos Toolkit (c.2003), and for her general eagerness to help. Finally, I wish to thank the School of Statistics and Actuarial Science at the University of the Witwatersrand for financing the purchase of the geostatistical add-on package S+SpatialStats (2001).

CONTENTS	Page
DECLARATION	ii
ABSTRACT	iii
ACKNOWLEDGEMENTS	iv
LIST OF FIGURES	ix
LIST OF TABLES	xix
LIST OF SYMBOLS AND COMMON NOTATION	xxii
CHAPTER ONE – INTRODUCTORY CHAPTER	1
1.1 Introduction	1
1.2 An Elementary Description of Geostatistics	6
1.3 The History and Development of Geostatistics	7
1.4 Plan and Purpose for this Dissertation	9
1.5 Justification for this Study	10
1.6 A Preview of the Chapters to Follow	11
1.7 The Spatial Data used in this Dissertation	14
CHAPTER TWO – GEOSTATISTICS AND THE MINING INDUSTRY	15
2.1 Introduction	15
2.2 Mining Terminology	16
2.3 The Application of Geostatistics in the Mining Industry	19
2.4 Statistical Considerations when Applying Geostatistics in the Mining Industry	20
2.4.1 Support and the support effect	20
2.4.2 Statistical distributions	23
2.5 The Mining Industry in South Africa	24
CHAPTER THREE – CLASSICAL STATISTICAL THEORY IN GEOSTATISTICS	26
3.1 Introduction	26
3.2 The Distribution of the Sample Population	27
3.2.1 Construction of the sample histogram	27

3.2.2	The declustering technique	28
3.3	The Distribution of the Measured Attribute over other Supports	29
3.3.1	The affine correction model	29
3.4	The Lognormal Distribution	30
3.4.1	The two-parameter lognormal distribution	30
3.4.2	The three-parameter lognormal distribution	38
3.5	Grade-Tonnage Curves	42

CHAPTER FOUR – THE THEORY OF REGIONALIZED VARIABLES 51

4.1	Introduction	51
4.2	The Probabilistic Model of Geostatistics	51
4.3	Assumptions	54
4.3.1	Second-order stationarity	54
4.3.2	Intrinsic stationarity	54
4.3.3	Ergodicity	55
4.4	Alternative Approaches to Spatial Estimation	57
4.4.1	Inverse distance weighting	57
4.4.2	Least squares regression	60
4.4.3	Polygonal estimation	61
4.4.4	Additional comments	63

CHAPTER FIVE – THE COVARIANCE FUNCTION AND THE VARIOGRAM 64

5.1	Introduction	64
5.2	Valid Covariance Functions and Variograms	65
5.3	Additional Properties of Covariance Functions and Semi-variograms	67
5.3.1	Mathematical properties	67
5.3.2	Continuity and differentiability	68
5.3.3	Behaviour near the origin	68
5.3.4	Behaviour further away from the origin	71
5.3.5	Isotropy and anisotropy	72
5.4	Commonly used Semi-variogram Models	76
5.4.1	The nugget effect model	77
5.4.2	The power model	77
5.4.3	The spherical model	78
5.4.4	The exponential model	79
5.4.5	The Gaussian model	79
5.4.6	Nested semi-variogram models	80

5.5	Estimation of the Semi-variogram	81
5.5.1	Method-of-moments estimator of the semi-variogram	81
5.5.2	The semi-variogram cloud	85
5.6	Fitting a Semi-variogram Model to the Estimated Semi-variogram . . .	86
5.7	Robust Estimates of the Semi-variogram	90
5.8	Relative Semi-variograms	91

CHAPTER SIX – EXPRESSIONS OF VARIANCE AND REGULARIZATION 93

6.1	Introduction	93
6.2	Estimation Variance	94
6.2.1	Extension variance	94
6.2.2	Estimating a block by a weighted average	97
6.3	Dispersion Variance	99
6.3.1	Krige’s relationship	101
6.4	Regularization	102
6.5	Calculation of $\bar{\gamma}(V, v)$	105
6.5.1	Discretization	105
6.5.2	Auxiliary functions	107
6.6	The Effect of Nested Semi-variogram and Covariance Structures on the Estimation Variance, Dispersion Variance and Regularization . . .	113

CHAPTER SEVEN – KRIGING 115

7.1	Introduction	115
7.1.1	The method of Lagrange multipliers for obtaining minima . . .	115
7.2	Ordinary Kriging	116
7.3	Simple Kriging	122
7.4	Kriging Weights	128
7.5	The Search Neighbourhood	136
7.6	Kriging as an Exact Interpolator	137
7.7	Kriging Variance	139
7.8	The Smoothing Effect	141
7.9	Cross Validation	142
7.10	Universal Kriging	143
7.11	Lognormal Kriging	149
7.12	Additional Issues in Kriging	153
7.12.1	Kriging using a relative (or proportional) semi-variogram model	153
7.12.2	Testing spatial data for the presence of trend	156

CHAPTER EIGHT – THE APPLICATION OF GEOSTATISTICAL THEORY	161
8.1 Introduction	161
8.2 Decisions Regarding the Semi-variogram	164
8.2.1 Deciding on the type of semi-variogram model	166
8.2.2 The use of robust semi-variogram models	172
8.3 The Choice of Spatial Estimator	176
8.4 Additivity and the Logarithmic Transformation of Spatial Data – Theory and Application	182
8.4.1 Additivity and accumulation	183
8.4.2 The logarithmic transformation of lognormally distributed spatial data	186
8.4.3 Geostatistical analysis of the supplied gold mining data set	188
CHAPTER NINE – THE PHILIP AND WATSON DEBATE	237
9.1 Introduction	237
9.2 Summary of the Philip and Watson Debate	237
9.3 Critical Examination of the Philip and Watson Debate	247
9.4 Drawing Conclusions from the Philip and Watson Debate	252
CHAPTER TEN – CONCLUDING CHAPTER	255
APPENDIX A – APPENDIX OF TABLES AND CHARTS	257
APPENDIX B – ELEMENTARY STATISTICS	261
B1 Basic Summary Statistics	261
B1.1 Measure of central tendency	261
B1.2 Measures of spread	262
B1.3 A measure of skewness	263
B1.4 A measure of ‘peakedness’	264
B2 The Normal (Gaussian) Distribution	266
APPENDIX C – THE MATHEMATICS OF POSITIVE AND NEGATIVE DEFINITENESS	269
REFERENCES	271

LIST OF FIGURES

Page

Figure 1.1	The location of the nine random variables $Z(1), Z(2), \dots, Z(9)$ in two-dimensional Euclidean space.	1
Figure 1.2	The relationship between $\rho \in (0,1)$ and $9^\#$. The dotted line clearly shows that for $\rho = 0.2$ the nine correlated random variables provide the same precision in estimation of the overall mean μ as would be provided by 5.61 independent random variables.	5
Figure 2.1	An illustration of the difference between the statistical and geological concept of a sample, taken from Wellmer (1998 : 1).	18
Figure 2.2	A comparison of the distributions of values based on point and block supports, taken from Wackernagel (1995 : 55). Notice that the two distributions have the same overall average value, but due to averaging, the variability of the block distribution is smaller than that of the point distribution.	21
Figure 2.3	The proportion above cut-off for point and block support, taken from Wackernagel (1995 :56). Because the point support distribution has a larger variability and because cut-off is above the mean, a larger proportion of point support observations than block support observations will exist above the cut-off value.	21
Figure 3.1	The probability density function of $X \sim \text{LN}(2, \sigma^2)$ for $\sigma = 0.25, 0.5, 0.75$ and 1.00 . This figure has been taken from Hogg & Tanis (1997 : 223) and shows the various shapes of the two-parameter lognormal distribution. It also illustrates that σ^2 is a good measure of spread of the lognormal distribution.	32
Figure 3.2	‘Grade-tonnage’ type curve displaying graphically the information contained in Table 3.1.	47

Figure 4.1	The location of the seven measured point support samples, as well as the location of the point to be estimated (which is indicated by the arrow). Figure 4.1 has been taken directly from Isaaks & Srivastava (1989 : 251).	58
Figure 5.1	Some common behaviours of semi-variograms near the origin. From left to right: parabolic behaviour; linear behaviour; discontinuity at the origin; pure nugget effect. Figure 5.1 is taken from Journel & Huijbregts (1978 : 39). . .	70
Figure 5.2	A typical semi-variogram function displaying a sill and a range. This figure has been taken from Armstrong (1998 : 26).	71
Figure 5.3	The example of geometric anisotropy and its elimination, as taken from Goovaerts (1997 : 91).	74
Figure 5.4	The example of zonal anisotropy and its elimination, as taken from Goovaerts (1997 : 94).	75
Figure 5.5	Basic shape of the nugget effect semi-variogram model.	77
Figure 5.6	The basic shape of the power semi-variogram models for a) $r = 1$ and b) $r < 1$ and $r > 1$	78
Figure 5.7	The basic shape of the spherical semi-variogram model.	78
Figure 5.8	The basic shape of the exponential semi-variogram model. . .	79
Figure 5.9	The basic shape of the Gaussian semi-variogram model.	80
Figure 5.10	A flowchart by Armstrong (1998 : 49) demonstrating the procedure followed for obtaining a method-of-moments semi-variogram estimate.	83
Figure 5.11	Plots of the four directional method-of-moments semi-variogram estimates. These plots have been taken from Armstrong (1998 : 51).	85

Figure 5.12	The isotropic method-of-moments estimate of the semi-variogram. Armstrong (1998 : 52) mentions that “a linear [semi-variogram] model with a ... nugget effect of about 3 gives a good fit [to this estimated semi-variogram].”	85
Figure 5.13	An example of a semi-variogram cloud taken from Wackernagel (1995).	86
Figure 5.14	a) A spherical semi-variogram model and b) a nested exponential semi-variogram model fitted to an experimental Cr concentration semi-variogram. Both models fit the experimental semi-variogram reasonably well. This figure is taken from Goovaerts (1997 : 100).	89
Figure 6.1	With $v \subset V$, this figure displays just some of the blocks of volume v that would be contained within the ‘block’ $V(x)$. . .	99
Figure 6.2	The point and regularized semi-variograms defined over a particular spatial region. Notice that for the larger modulus values of the vector h , the two semi-variograms simply differ in value by $\bar{\gamma}(v, v)$. This diagram has been taken from Journel & Huijbregts (1978 : 78).	104
Figure 6.3	The point support semi-variogram model for the metal accumulation in Example 6.1. This diagram is taken from Rendu (1981 : 30).	106
Figure 6.4	The 3×3 grid placed over the block $V(x)$ in Example 6.1. This diagram is also taken from Rendu (1981 : 30).	107
Figure 6.5	A line segment AB of length L . This figure is taken from Journel & Huijbregts (1978 : 108).	107
Figure 6.6	Rectangle $ABCD$ with sides of length L and l . This figure is taken from Journel & Huijbregts (1978 : 109).	108
Figure 6.7	Visual summary of the four auxiliary functions defined in two dimensions. This figure has been taken from Rendu (1981 : 31), and the letters z' and z'' represent the two extremities of the vector h	110
Figure 6.8	The location of the point support sample $z(x)$ and the block V .	111

Figure 7.1	The data configuration of the five samples and the block to be estimated.	121
Figure 7.2	Situation 1: The location of the five point support samples $\{z(x_i): i = 1 \text{ to } 5\}$ and the point to be estimated $z(x_0)$	130
Figure 7.3	Situation 2: The location of the five point support samples $\{z(x_i): i = 1 \text{ to } 5\}$ and the point to be estimated $z(x_0)$	130
Figure 7.4	It is mentioned that the isotropic spherical covariance model in Equation 7.15 possesses a zero nugget effect and a unit sill. Now by introducing various nugget effect values, it can be seen how the ordinary kriging weights for the data configuration in Figure 7.3 are affected. The behaviour of the kriging weights discussed in the preceding paragraph is clearly displayed in this figure. Notice that when the entire unit sill is taken up by the nugget effect, all the kriging weights converge. The idea behind Figure 7.4 was taken from Goovaerts (1997 : 177).	133
Figure 7.5	The location of five point support samples $\{z(x_i): i = 1 \text{ to } 5\}$ that will be used to estimate the point random variable $Z(x_0)$ via ordinary kriging. Note that in this illustration, the location x_0 is exactly the same as the location x_1 (i.e. the point to be estimated is located at the exact same point as one of the available samples).	138
Figure 7.6	The estimation of point A via kriging for two situations: one having consistent data values, the other having highly variable data values. Note that the data configuration of each of these situations is identical.	140
Figure 7.7	Example 7.3: Location of the five point support samples and the point to be estimated.	154
Figure 7.8	Plots associated with the example taken from Kaluzny et al. (1998). This figure is taken from Kaluzny et al. (1998 : 38).	157
Figure 7.9	A linear regression surface fitted to the available sample values. This figure is taken from Clark & Harper (2000 : 177).	158
Figure 7.10	Scatter-plot displaying the location and the relative value of the available samples.	159

Figure 7.11	The semi-variogram from Clark & Harper (2000 : 226) displaying a parabolic increase from a lag distance of about seventy meters.	159
Figure 8.1	Contour plot of the simulated regionalized variable possessing the underlying Gaussian semi-variogram.	166
Figure 8.2	Contour plot of the simulated regionalized variable possessing the underlying spherical semi-variogram.	166
Figure 8.3	The isotropic experimental semi-variogram of the simulated data set containing 144 point support samples.	167
Figure 8.4	The Fitted Gaussian semi-variogram model.	168
Figure 8.5	The fitted spherical semi-variogram model.	168
Figure 8.6	The ordinary kriging prediction surface assuming the Gaussian semi-variogram model in Figure 8.4.	169
Figure 8.7	The ordinary kriging prediction surface assuming the spherical semi-variogram model in Figure 8.5.	169
Figure 8.8	A spherical semi-variogram model with a nugget effect fitted to the experimental semi-variogram displayed in Figure 8.3.	171
Figure 8.9	The ordinary kriging prediction surface assuming the nugget inclusive spherical semi-variogram model in Figure 8.8.	171
Figure 8.10	Histogram of the 144 point support values of the simulated spatial data set introduced in Section 8.2.1.	172
Figure 8.11	Histogram of the 144 point support values of the simulated spatial data set introduced in Section 8.2.1 after two of the values were replaced by larger outlying values. These two outliers can clearly be seen in this histogram.	173
Figure 8.12	The experimental semi-variogram of the simulated data set with two of the 144 values replaced by larger outliers.	174

Figure 8.13	The robust experimental semi-variogram of the outlier inclusive simulated data set, together with a fitted spherical semi-variogram model (cf. Figure 8.5).	176
Figure 8.14	Histogram of the 94 true values.	178
Figure 8.15	Histogram of the 94 polygonal estimates.	178
Figure 8.16	Histogram of the 94 inverse distance weighting estimates.	178
Figure 8.17	Histogram of the 94 ordinary kriging estimates.	178
Figure 8.18	Histogram of the estimation errors associated with the polygonal estimates.	180
Figure 8.19	Histogram of the estimation errors associated with the inverse distance weighting estimates.	180
Figure 8.20	Histogram of the estimation errors associated with the ordinary kriging estimates.	180
Figure 8.21	The spatial location of all 2321 point support gold-ore samples.	183
Figure 8.22	The spatial location of the 2321 point support samples of the gold mining data set provided by Dr. Dohm. The 384 red-coloured points represent the samples that will be removed from this data set. These samples are located in six distinct zones (or blocks, see Note 8.12). The remaining 1937 black-coloured samples will be used to re-estimate the gold grade at the location of each of the removed (red-coloured) samples.	190
Figure 8.23	Histogram of the gold-ore grade of the 1937 point support samples.	191
Figure 8.24	Histogram of gold-ore thickness of the 1937 point support samples.	191
Figure 8.25	Histogram of the gold-ore accumulation of the 1937 point support samples.	191

Figure 8.26	A histogram of the available 1937 $\ln[y(x)]$ values. The histogram displays a skewness of 0.04 and a kurtosis of 2.73.	199
Figure 8.27	The isotropic nested spherical semi-variogram model fitted to the experimental semi-variogram calculated from the 1937 $\ln[y(x)]$ values. This semi-variogram model is a combination of two spherical semi-variogram models, and also displays a relatively large nugget effect. Note that the size of the symbols \oplus is proportional to the number of sample pairs used to obtain that point.	200
Figure 8.28	A histogram of the available 1937 $\ln[u(x)]$ values. The histogram displays a skewness of 0.04 and a kurtosis of 2.57.	202
Figure 8.29	The isotropic nested exponential semi-variogram model fitted to the experimental semi-variogram calculated from the 1937 $\ln[u(x)]$ values. This semi-variogram model is a combination of two exponential semi-variogram models, and also displays a relatively large nugget effect. Note again that the size of the symbols \ominus is proportional to the number of sample pairs used to obtain that point.	202
Figure 8.30	The cubic trend surface over the ore deposit, fitted to the 1937 gold-ore thickness values by Geostokos Toolkit (c.2003).	203
Figure 8.31	The isotropic spherical semi-variogram model fitted to the experimental semi-variogram calculated from the 1937 cubic surface residuals of the gold-ore thickness.	204
Figure 8.32	The isotropic experimental semi-variogram calculated from the 1937 untransformed gold-ore grade sample values.	205
Figure 8.33	The spatial study area (i.e. the gold-ore deposit), which contains 1937 point support sample values (represented by the grey dots), is divided into nine non-overlapping rectangular zones in order to test for the presence of a proportional effect. All nine zones are of equal size and measure 150 Eastings x 175 Northings.	206
Figure 8.34	Scatterplot of the local mean versus the local standard deviation for each of the nine zonal areas in Figure 8.33 (see Table 8.5). The correlation between the local mean and the local standard deviation is calculated as 0.89.	207

Figure 8.35	The nine experimental gold-ore grade semi-variograms for each of the nine non-overlapping zones (see Figure 8.33) and the local relative gold-ore grade experimental semi-variogram calculated from these nine experimental semi-variograms. . .	208 to 210
Figure 8.36	The nested exponential semi-variogram model fitted to the local relative experimental semi-variogram.	210
Figure 8.37	Scatterplot of the local gold-ore accumulation mean versus the local gold-ore accumulation standard deviation for each of the nine zonal areas in Figure 8.33. The correlation between the local mean and the local standard deviation is calculated as 0.76.	212
Figure 8.38	The nine experimental gold-ore accumulation semi-variograms for each of the nine non-overlapping zones in Figure 8.33, and the local relative gold-ore accumulation experimental semi-variogram calculated from these nine experimental semi-variograms.	214 and 215
Figure 3.39	The nested exponential semi-variogram model fitted to the local relative experimental semi-variogram in Figure 8.38. . .	216
Figure 8.40	The isotropic nested exponential semi-variogram model fitted to the experimental semi-variogram calculated from the 1937 available gold-ore grade values. This semi-variogram model is a combination of two exponential semi-variogram models, and also displays a nugget effect.	217
Figure 8.41	The isotropic nested exponential semi-variogram model fitted to the experimental semi-variogram calculated from the 1937 gold-ore accumulation values. This semi-variogram model is a combination of two exponential semi-variogram models, and also displays a nugget effect.	219
Figure 8.42	A histogram showing the true gold-ore grade distribution of the 384 point support samples that are to be re-estimated by each of the six geostatistical analyses.	220
Figure 8.43	a) A histogram of the 384 point support gold-ore grade estimates produced by Geostatistical Analysis 1, and b) A histogram of the 384 estimation errors (i.e. the true gold-ore grade less the estimated gold-ore grade), associated with Geostatistical Analysis 1.	221

Figure 8.44	a) A histogram of the 384 point support gold-ore grade estimates produced by Geostatistical Analysis 2, and b) A histogram of the 384 estimation errors (i.e. the true gold-ore grade less the estimated gold-ore grade), associated with Geostatistical Analysis 2.	221
Figure 8.45	a) A histogram of the 384 point support gold-ore grade estimates produced by Geostatistical Analysis 3, and b) A histogram of the 384 estimation errors (i.e. the true gold-ore grade less the estimated gold-ore grade), associated with Geostatistical Analysis 3.	221
Figure 8.46	a) A histogram of the 384 point support gold-ore grade estimates produced by Geostatistical Analysis 4, and b) A histogram of the 384 estimation errors (i.e. the true gold-ore grade less the estimated gold-ore grade), associated with Geostatistical Analysis 4.	222
Figure 8.47	a) A histogram of the 384 point support gold-ore grade estimates produced by Geostatistical Analysis 5, and b) A histogram of the 384 estimation errors (i.e. the true gold-ore grade less the estimated gold-ore grade), associated with Geostatistical Analysis 5.	222
Figure 8.48	a) A histogram of the 384 point support gold-ore grade estimates produced by Geostatistical Analysis 6, and b) A histogram of the 384 estimation errors (i.e. the true gold-ore grade less the estimated gold-ore grade), associated with Geostatistical Analysis 6.	222
Figure 8.49	Scatterplots of the logarithms of the 384 estimated gold-ore grades versus the logarithms of the associated 384 true gold-ore grades, for each of the six geostatistical analyses.	227
Figure 8.50	Scatterplot of the logarithms of the 384 estimated gold-ore grades versus their associated 384 estimation errors for Geostatistical Analysis 2. The larger estimates are often associated with large positive errors. This is a direct consequence of the smoothing effect on the kriging estimates and the skew distribution of the true gold-ore grade values in Figure 8.42.	228

Figure A1	A chart for the auxiliary function $H(L ; l)$ of a spherical semi-variogram model with a sill and range value equal to one. The letter a in the axes refers to the range parameter of the non-standardized spherical semi-variogram model (see Equation 5.14). This chart is taken from Journel & Huijbregts (1978 : 127).	260
Figure B1	An example of a positively skew, symmetric and negatively skew distribution.	264
Figure B2	An example of a leptokurtic and a platykurtic distribution. . .	265
Figure B3	A normal probability distribution with mean μ and standard deviation σ^2 , taken from Clark & Harper (2000 : 32).	266

WITSETD

LIST OF TABLES	Page
Table 2.1 South Africa’s mineral reserves, 2001 (from Burger, c.2003).	25
Table 3.1 Table showing the proportion of the polluted area above the pollution cut-off level as well as the average pollution value of these regions, for a number of possible pollution cut-off values.	47
Table 4.1 Inverse distance weighting calculations for estimating the point $z(x_0)$, using the seven available sample values in Figure 4.1.	59
Table 4.2 The regression equation fitted to describe the proportion of pyritic sulphur in a certain type of coal (taken from Armstrong, 1998 : 17).	61
Table 5.1 The location of all sixty four values. This table is taken from Armstrong (1998 : 51).	84
Table 5.2 Calculations of $\hat{\gamma}(h)$ for various distances and directions, for the data in Table 5.1. The values in this table were taken directly from Armstrong (1998 : 51). Note that the values $N(h)$ correspond to the number of sample pairs associated with each of the lag distances h (see Equation 5. 19).	84
Table 5.3 Calculation of the isotropic semi-variogram values $\hat{\gamma}(h)$ for various distances, for the data in Table 5.1.	85
Table 8.1 Summary of the distribution of the 94 true values, the 94 polygonal estimates, the 94 inverse distance weighting estimates, and the 94 ordinary kriging estimates.	178
Table 8.2 Summary of the estimation error distribution associated with the polygonal estimation, inverse distance weighting estimation and ordinary kriging estimation.	180
Table 8.3 Summary statistics of gold-ore grade, gold-ore thickness and gold-ore accumulation of the 1937 point support samples. . .	192

Table 8.4	Summary of the assumptions of the six geostatistical analyses.	197
Table 8.5	A table giving the local mean and the local standard deviation of gold-ore grade values within each zone, as well as the number of samples contained within each zone.	206
Table 8.6	Table giving the local mean and the local standard deviation of the gold-ore accumulation sample values within each zone, as well as the number of samples contained within each zone.	212
Table 8.7	Various summary statistics calculated for each of the six geostatistical analyses.	224
Table 8.8	Ranking of the performance of the six geostatistical analyses for each of the seven summary statistics presented in Table 8.7. A ranking of one is associated with the geostatistical analysis that performed the best with respect to the measured statistic; a ranking of six is associated with the geostatistical analysis that performed worst. The final row in this table gives the sum of the rankings for each of the geostatistical analyses.	229
Table 8.9	A summary of the relative performance of the six geostatistical analyses with respect to the sum of the rankings (see Table 8.8), the median squared error, and the median absolute error (see Table 8.7).	231
Table 8.10	Summary of the conclusions drawn from the comparison of the six geostatistical analyses in Section 8.4.3.	234
Table 8.11	Mean and median average percentage error calculated for each of the six geostatistical analyses studied in Section 8.4.3.	236
Table A1	Table of $\gamma_n(V_y)$ for various values V_y and n , taken from Sichel (1966 : 117-118).	257
Table A2	Table of $\psi_{0.05}(V_y, n)$ and $\psi_{0.95}(V_y, n)$, taken from Sichel (1966 : 119).	258
Table A3	Cumulative distribution of the standard normal distribution taken from Hogg & Tanis (1997).	259

Table A4 Various values of the auxiliary function $H(L;B)$ for a spherical model with sill and range value equal to one. This table is taken from Clark (1979 : 82). 260

WITSETD

LIST OF SYMBOLS AND COMMON NOTATION

	indicate the conclusion of a proof
	indicates the conclusion of an example
	indicates the conclusion of a note
$\alpha(L ; l)$	an auxiliary function
β	the threshold parameter of a three-parameter lognormal distribution
β_1	the square of the population skewness
β_2	the population kurtosis
c_0	a nugget-effect
$C(0)$	the covariance value at a lag of zero; equal to the variance of a second-order stationary random function
$C(h)$	a covariance function
$\chi(L)$ and $\chi(L ; l)$	auxiliary functions
$C_V(h)$	the regularized covariance function of support V , i.e. the covariance function of a random function of support V
$\bar{C}(V, v)$	the mean value of $C(h)$ when one extremity of vector h describes the domain $V(x)$ and the other extremity independently describes the domain $v(y)$
$C(x,y)$ or $\text{cov}(x,y)$	the covariance between the random variables $Z(x)$ and $Z(y)$

$D^2(v/V)$	the dispersion variance of blocks $v(y)$ within $V(x)$
$E\{Z(x)\}$	the expectation of a random function or a random variable
$F(L)$ and $F(L ; l)$	auxiliary functions
$f(x)$	generally indicates a function of the spatial co-ordinate x , or a probability density function
$\gamma(h)$	a semi-variogram. $2\gamma(h)$ is the notation for a variogram.
$\gamma_r(h)$	the regularized semi-variogram of support V , i.e. the semi-variogram of a random function of support V
$\gamma(x,y)$	the semi-variogram value between the random variables $Z(x)$ and $Z(y)$
$\bar{\gamma}(V, v)$	the mean value of $\gamma(h)$ when one extremity of the vector h describes the domain $V(x)$ and the other extremity independently describes the domain $v(y)$
h	a separation vector of modulus $\ h\ $
$H(L ; l)$	an auxiliary function
$\lambda_i, \lambda_j, \dots$	generally refers to kriging weights or the weights of a linear combination
μ	the population mean
$N(h)$	indicates the set containing all sample pairs separated by the vector h
OK	ordinary kriging
OLK	ordinary lognormal kriging
Ω	a spatial study area of two- or three-dimensions

$\Phi(y)$	the cumulative distribution function of the standard normal distribution
$1, 2, 3$	one-, two- and three dimension Euclidean space respectively
σ^2	the population variance
σ_E^2	the estimation variance
$\sigma_E^2(v, V)$	the extension variance of v to V
σ_{OK}^2	the ordinary kriging variance
σ_{OLK}^2	the ordinary lognormal kriging variance
σ_{SK}^2	the simple kriging variance
σ_{UK}^2	the universal kriging variance
SK	Simple kriging
t	Sichel's t-estimator
τ	the mean value of a two- or three-parameter lognormal distribution
UK	universal kriging
$\text{var}\{Z(x)\}$	the variability of a random function or a random variable
$V(x)$	A volume (or area) V centred at the point location x
$v(x)$	a volume (or area) v , usually smaller than V , centred at the point location x
ϖ, ϖ_i	Lagrange multipliers
x, y, \dots	generally indicates a point co-ordinate in one-, two- or three-dimensional space

- $Z_V(x)$ a block support random function or random variable, with a support volume (or area) of V
- $z_V(x)$ a block support regionalized variable or a realization of a block support random variable, with a support volume (or area) of V
- $Z(x), Y(x), \dots$ a random function or a random variable at the point location x
- $z(x), y(x), \dots$ a regionalized variable or a realization of a random variable at the point location x

WILEY